GEOPHYSICAL RESEARCH LETTERS, VOL. 37, L14308, doi:10.1029/2010GL044205, 2010

Fundamentals of elasticity of $(Mg_{1-x}, Fe_x)_2SiO_4$ olivine

M. Núñez-Valdez,[1] K. Umemoto,[2] and R. M. Wentzcovitch[3]

Received 4 June 2010; accepted 16 June 2010; published 24 July 2010.

[1] We study the influence of iron on the elasticity of $(Mg_{1-x}, Fe_x)_2SiO_4$ olivine ($0 \le x \le 0.125$), a major constituent of the Earth's upper mantle. We calculate static elastic properties by first principles for this solid solution and investigate the effect of atomic arrangement, an artifact of supercell calculations, on all single crystal and poly-crystalline elastic moduli. From calculated wave propagation velocities we find the heterogeneity ratios of shear to compressional wave velocity, and bulk sound to shear wave velocity. Their values are, though limited to composition considerations, marginally consistent with seismic tomography. **Citation:** Núñez-Valdez, M., K. Umemoto, and R. M. Wentzcovitch (2010), Fundamentals of elasticity of $(Mg_{1-x}, Fe_x)_2SiO_4$ olivine, *Geophys. Res. Lett.*, *37*, L14308, doi:10.1029/2010GL044205.

1. Introduction

[2] Olivine $(Mg_{1-x}, Fe_x)_2SiO_4$ is the most abundant phase of the Earth's upper mantle (<410 km) [*Rinwood*, 1975; *Putnis*, 1992]. Experimentally, the elastic constants of olivine and its end-member forsterite (Mg_2SiO_4) have been investigated at mantle pressures by methods such as impulsive stimulated scattering [*Abramson et al.*, 1997], Brillouin scattering [*Zha et al.*, 1996, 1998], and ultrasonic interferometry [*Chen et al.*, 1996; *Liu et al.*, 2005]. Knowledge of the elastic properties of the upper mantle minerals is of great importance for interpretation of seismic data. In particular, the anisotropy of olivine could help us understand seismic anisotropy and flow geometry in this region [*Mainprice et al.*, 2005]. The pressure dependence of the static elastic constants of Mg_2SiO_4 forsterite has been predicted by first-principles [*da Silva et al.*, 1997]; but, to the best of our knowledge, elastic properties of olivine have not been calculated. To address the effect of iron on the elasticity of orthorhombic olivine (space group Pbnm [*Hazen*, 1976]) we calculate the structure, equation of state, and the full static elastic constant tensor C_{ij} of $(Mg_{1-x},Fe_x)_2SiO_4$ for $x = 0$ and $x = 0.125$ between 0 and 20 GPa, a range that includes upper mantle pressures. From the elastic constants we determine seismic wave velocities and anisotropy in the single crystal and in fully isotropic and transversely isotropic aggregates. From our results we get an overall perspective of the effect of iron on the elastic properties of olivine.

2. Theory

[3] Our first-principles calculation is based on Density Functional Theory (DFT) [*Hohenberg and Kohn*, 1964; *Kohn and Sham*, 1964]. We adopt the Local Density Approximation (LDA) for the exchange-correlation energy functional [*Ceperley and Alder*, 1980]. This produces a small gap insulator with correct orbital occupancies $(Mg_{1-x},Fe_x)_2SiO_4$ for $x = 0.125$. Therefore, there is no need for LDA + U/GGA + U-type calculations in the structural properties as discussed by H. Hsu et al. (The Hubbard U correction and iron-bearing minerals: Discussion of "Determination of the high-pressure properties of fayalite from first-principles calculations" by S. Stackhouse, L. Stixrude, and B. Karki, submitted to *Earth and Planetary Science Letters*, 2010). The pseudopotential for Mg was generated by von Barth-Car's method. For Fe, Si, and O, we use pseudopotentials generated by Vanderbilt's method [*Vanderbilt*, 1990]. The plane-wave cutoff energy is 40 Ry and a $4 \times 2 \times 4$ k-point mesh is used for the Brillouin zone sampling.

[4] We optimize a 28-atom unit cell of $(Mg_{1-x}, Fe_x)_2SiO_4$ at six different pressures up to 20 GPa. Such structural optimization uses a variable cell shape molecular dynamics strategy [*Wentzcovitch*, 1991; *Wentzcovitch et al.*, 1993] to obtain the ground state atomic configuration in equilibrium at arbitrary pressures.

[5] For pressures <15 GPa, high spin (HS) iron in olivine has the lowest enthalpy. Beyond 15 GPa, the low spin (LS) state has lower enthalpy than the HS state, indicating a spin transition. Experimentally this HS to LS crossover was suggested to occur between 40 and 50 GPa [*Rouquette et al.*, 2008]. Also the HS-LS transition in olivine at pressures ~70 GPa was suggested to account for a distinct layered structure in Earth's lower mantle via iron partitioning and depletion [*Irifune et al.*, 2010]. Our underestimation of the spin transition pressure is due to LDA [*Umemoto et al.*, 2008]. Therefore we constrain iron in the HS state between 15 and 20 GPa to have HS in the full interval pressure 0–20 GPa.

[6] Forsterite has two types of Mg sites: M(1) and M(2) [*Hazen*, 1976]. Thus we consider two ways to incorporate iron: Fe → M(1) and Fe → M(2). That is, a Fe-atom is placed in one of the four M(1) or M(2) equivalent sites in the 28-atom unit cell, corresponding to $x = 0.125$. Experimentally, olivine has orthorhombic symmetry (Pbnm), implying a disordered Mg-Fe arrangement. However, the calculated elastic constants belong to a particular Mg-Fe arrangement with lowered (monoclinic) symmetry under hydrostatic compression (homogeneous stress). Therefore, to obtain the elastic constants for the fully disordered orthorhombic

[1]School of Physics and Astronomy, University of Minnesota-Twin Cities, Minneapolis, Minnesota, USA.
[2]Department of Geology and Geophysics, University of Minnesota-Twin Cities, Minneapolis, Minnesota, USA.
[3]Department of Chemical Engineering and Materials Science, Minnesota Supercomputing Institute, University of Minnesota-Twin Cities, Minneapolis, Minnesota, USA.

0094-8276/10/2010GL044205

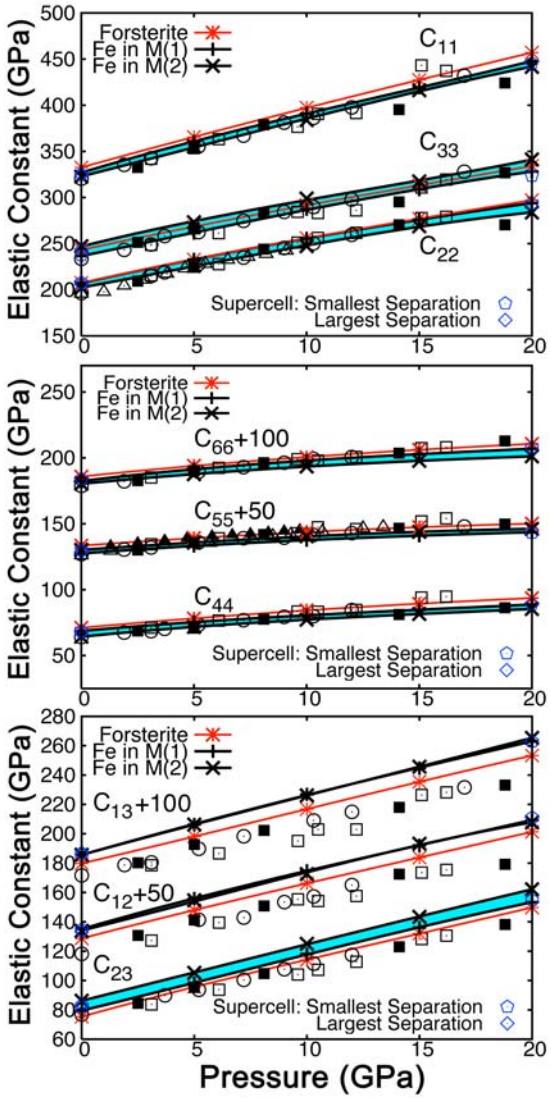

Figure 1. Lines (red: $x = 0$, black: $x = 0.125$) are cubic polynomial fits of our calculated C_{ij} [color regions are spanned between curves of olivine with Fe in M(1) or M(2)] compared with experiments by *Abramson et al.* [1997], open circles ($x = 0.1075$) [*Zha et al.*, 1996, 1998]; open squares ($x = 0$), solid squares ($x = 0.1$) [*Chen et al.*, 1996]; open triangles ($x = 0$); solid triangles ($x = 0.1$).

system, we average over the possible symmetrically equivalent positions of the Fe atom:

$$S_{ijkl} = \frac{1}{4}\sum_{s=1}^{4} R^s_{im} R^s_{jn} R^s_{ko} R^s_{lp} \tilde{S}_{mnop} \qquad (1)$$

where R^s are the point group symmetry operations that relate the four symmetrically equivalent M(1) or M(2) sites to each other (including the identity), and $\tilde{S} = (\tilde{C})^{-1}$ are the computed compliance constants. In this way, the final elastic tensor, $C_{ijkl} = (S_{ijkl})^{-1}$ (or C_{ij} in the Voigt notation [*Wallace*, 1972]), has the appropriate Pbnm symmetry. We symmetrize the compliance's tensor instead of the elastic constant's tensor [*Kiefer et al.*, 2002] in the spirit of the Reuss average that corresponds to homogeneous stress. To determine $\tilde{C}$ at a given pressure, the equilibrium cell is strained, and the internal parameters are re-relaxed. We apply positive and negative strains of magnitude 1% in order to obtain accuracy in the limit of zero strain. This procedure was used on several solids and mantle silicates [*Wentzcovitch et al.*, 1995; *Karki et al.*, 1997].

3. Results and Discussion

[7] The static elastic constants of forsterite and olivine are shown in Figure 1 and Table 1. They are slightly larger than experimental values but in good agreement with them. The theoretical elastic constants tend to be overestimated by the static LDA calculation. The elastic constants C_{ij} for $0 \le x \le 0.125$ increase monotonically and almost sublinearly with pressure, for $i, j \le 3$. Experimentally, C_{44}, C_{55}, and C_{66} also show a non-linear pressure dependence [*Abramson et al.*, 1997; *Zha et al.*, 1996, 1998; *Chen et al.*, 1996]. The effect of iron on C_{ij} can be summarized as follows: by increasing x from 0 to 0.125, off-diagonal C_{ij} increase by 5.5–7%, shear C_{ij} decrease by 6–7%, C_{33} is unaffected, and C_{11} and C_{22} decrease by ~3%. In addition to the 28-atom unit cell, we also investigate a 56-atom supercell for two other atomic configurations: with two irons as far apart as possible (at 0 GPa) and with two neighboring irons (at 0 and 20 GPa). These configurations produce C_{ij}, in both cases, within the range of C_{ij} from the 28-atom cell.

[8] The isotropically averaged bulk (K) and shear (G) moduli are calculated using the Voigt-Reuss-Hill averaging scheme [*Watt*, 1979] (Figure 2a). For $x = 0.125$, in average the bulk modulus increases by 2.2% at zero pressure and 1.5% at 20 GPa. The impact of iron on the shear modulus is stronger. With respect to forsterite, G in olivine decreases by ~6.0% throughout the pressure interval investigated. Experiments also show an increase in bulk modulus and a decrease in shear modulus for olivine with respect to forsterite up to 15 GPa [*Abramson et al.*, 1997; *Zha et al.*, 1996, 1998]. Moreover, *Speziale et al.* [2004] also indicated this trend for the full range $0 \le x \le 1$.

[9] Figure 2b shows the isotropic average compressional (P), shear (S) and bulk (Φ) wave velocities [*Poirier*, 2000],

$$V_P = \sqrt{\frac{K + \frac{4}{3}G}{\rho}}, \quad V_S = \sqrt{\frac{G}{\rho}}, \quad V_\Phi = \sqrt{\frac{K}{\rho}}, \qquad (2)$$

Table 1. Elastic Moduli (GPa) for *a*: $x = 0$; *b*: $x = 0.125$ Fe in M(1) and *c*: $x = 0.125$ Fe in M(2) at 0 and 20 GPa[a]

P	C_{11}	C_{22}	C_{33}	C_{44}	C_{55}	C_{66}	C_{12}	C_{13}	C_{23}	K	G
0^a	332.5	207.6	243.0	70.9	83.3	85.7	78.8	79.6	76.5	136.8	83.3
0^b	327.7	207.3	236.3	68.6	77.4	82.7	85.4	86.0	79.6	139.0	79.4
0^c	322.6	202.0	247.9	64.2	80.1	80.2	83.9	86.0	86.5	140.6	78.0
20^a	457.1	297.1	334.2	93.6	100.1	110.7	151.3	153.4	149.5	218.5	101.7
20^b	447.6	294.0	328.1	88.8	93.6	106.8	159.3	162.9	153.4	221.0	96.1
20^c	442.0	284.0	340.7	85.4	96.2	101.2	158.0	165.3	162.0	222.8	93.8

[a] K and G are calculated as Voigt-Reuss-Hill averages.

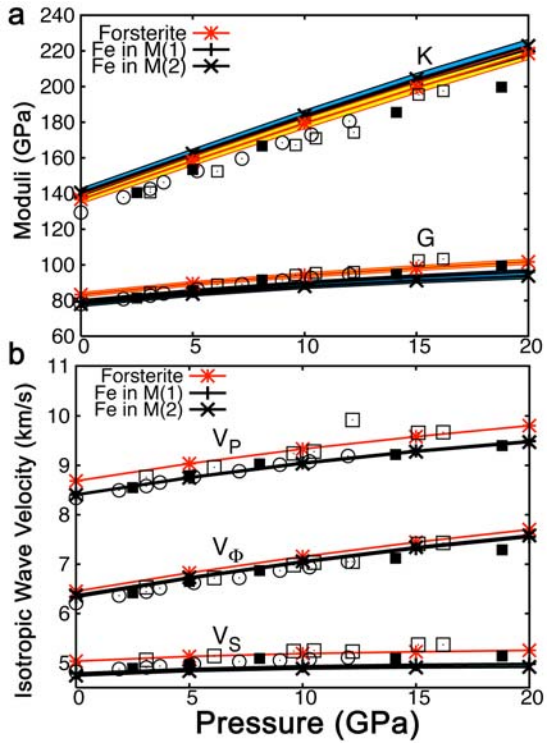

Figure 2. Pressure dependance of the aggregate properties of $(Mg_{1-x}, Fe_x)_2SiO_4$ (red lines: $x = 0$, black lines: $x = 0.125$) compared to experimental data from *Abramson et al.* [1997] open circles ($x = 0.1075$) [*Zha et al.*, 1996, 1998]; open squares ($x = 0$); solid squares ($x = 0.1$). (a) Bulk and shear moduli: color regions are given by the Voigt-Reuss-Hill upper and lower limits. (b) Compressional, shear, and bulk isotropic wave velocities.

where ρ is the density. In the pressure range considered, V_P decreases by ~3.3% when x varies from 0 to 0.125, while V_S decreases by ~6.3%.

[10] Elastic anisotropy and its pressure dependance are important to understand seismic anisotropies in terms of mantle flow geometry. In order to study wave velocity anisotropy, we solve the Christoffel equation [*Musgrave*, 1970] for acoustic velocities in single crystal:

$$\det\left|C_{ijkl}n_jn_l - \rho v^2\delta_{ik}\right| = 0. \tag{3}$$

In equation (3), v is elastic wave velocity, **n** is propagation direction, δ_{ij} is Kronecker delta, and ρ is density. For a given **n**, there are three solutions corresponding to one P-wave and two S-waves. The calculated wave velocities of olivine are smaller than those of forsterite. This is expected because Fe is heavier than Mg. We find that the directional dependance of P- and S-wave velocities for $x = 0$ and $x = 0.125$ are qualitatively similar between 0 and 20 GPa. The directions of fastest and slowest propagation for P-waves are [100] and [010], respectively. The fastest S-waves propagate in the [101] direction for all pressures, the slowest directions change from [010] and [001] at 0 GPa to approximately [011] at ~5 GPa and up to 20 GPa. The direction of maximum difference between the S-waves velocities changes from [101] at zero pressure to approximately [011] at 20 GPa, that is, from the fastest to the slowest propagation direction.

[11] The magnitudes of azimuthal anisotropy for P- (A_P) and S- (A_S) waves in the single crystal (Figure 3a) are [*Wentzcovitch et al.*, 1998]:

$$A_P = \left(\frac{v_{P\max} - v_{P\min}}{V_P}\right) \times 100, \text{ and } A_S = \left(\frac{v_{S\max} - v_{S\min}}{V_S}\right) \times 100, \tag{4}$$

where V_P and V_S are the aggregate velocities. In the pressure interval relevant for the upper mantle, A_P decreases monotonically. Meanwhile, A_S first decreases to a minimum at 5 GPa, then it increases monotonically.

[12] Polarization anisotropy of shear waves is described by:

$$A^{pol}_{[ijk]} = \frac{|v_{S_1} - v_{S_2}|}{V_S} \times 100, \tag{5}$$

where v_{S_1} and v_{S_2} are the two shear waves in the [ijk] direction. In Figure 3b we show the pressure dependance of $A^{pol}_{[ijk]}$ for the three main crystallographic directions: [100], [010], and [001]. For $x = 0$ and $x = 0.125$, directions [100] and [001] show steady increase and decrease polarization anisotropy, respectively, up to 20 GPa.

[13] Anisotropy in a transversely isotropic aggregate of $(Mg_{1-x}, Fe_x)_2SiO_4$ is also useful for interpretation of upper mantle anisotropy in terms of mantle flow. Transverse anisotropies of v_P and v_S are defined as:

$$A^T_P = \left(\frac{v_{PH} - v_{PV}}{V_P}\right) \times 100 \quad \text{and} \quad A^T_S = \left(\frac{v_{SH} - v_{SV}}{V_S}\right) \times 100, \tag{6}$$

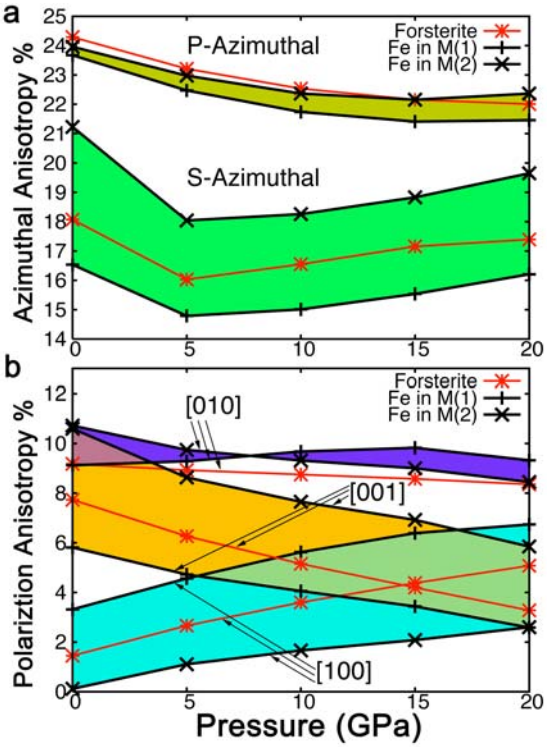

Figure 3. Pressure variation of (a) azimuthal and (b) polarization (for S-wave) anisotropy of elastic wave velocities of $(Mg_{1-x}, Fe_x)_2SiO_4$ (red lines: $x = 0$, black lines: $x = 0.125$, color regions indicate limits of Fe in M(1) or M(2)).

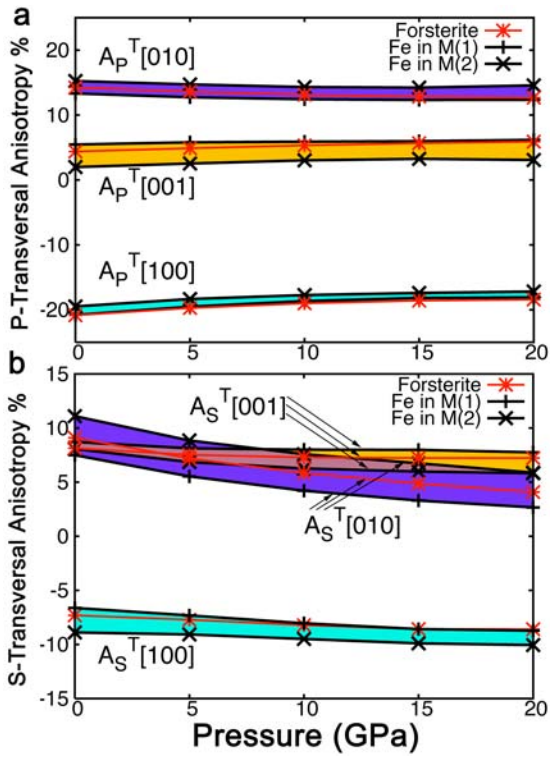

Figure 4. Pressure dependence of wave velocity anisotropy for a transversely isotropic aggregate of $(Mg_{1-x}, Fe_x)_2SiO_4$ with symmetry axis along [100], [010], and [001] directions (red lines: $x = 0$, black lines: $x = 0.125$, color regions indicate limits of Fe in M(1) or M(2)). (a) P-waves. (b) S-waves.

respectively, where $v_{PH} = \sqrt{\frac{A}{\rho}}\left(v_{PV} = \sqrt{\frac{C}{\rho}}\right)$ is the velocity of P-waves propagating horizontally (vertically), and $v_{SH} = \sqrt{\frac{N}{\rho}}\left(v_{SV} = \sqrt{\frac{L}{\rho}}\right)$ is the velocity of S-waves polarized horizontally (vertically). For a transversely isotropic medium with vertical symmetry axis [001]: $A = \frac{3}{8}(C_{11} + C_{22}) + \frac{1}{4}C_{12} + \frac{1}{2}C_{66}$, $C = C_{33}$, $N = \frac{1}{8}(C_{11} + C_{22}) - \frac{1}{4}C_{12} + \frac{1}{2}C_{66}$, and $L = \frac{1}{2}(C_{44} + C_{55})$. Cyclic permutations of Cartesian indices are used for the [100] and [010] symmetry axes [*Wentzcovitch et al.*, 1998].

[14] These transverse anisotropies for aggregates with *a*, *b*, and *c* axes aligned vertically are shown in Figure 4. For vertically oriented [010] and [001] axes, A_P^T is always positive and almost independent of pressure in the interval of 0–20 GPa. For vertically oriented [100] symmetry axis, P-waves propagate faster (slower) when parallel (perpendicular) to it, therefore, anisotropy is always negative between 0 and 20 GPa. This is understood from the elastic constant C_{11} being larger than their counterpart $\frac{3}{8}(C_{22} + C_{33}) + \frac{1}{4}C_{23} + \frac{1}{2}C_{44}$. Similarly, vertically polarized waves are faster than horizontally polarized waves resulting in $A_S^T < 0$. The transverse anisotropy of S-waves with [010] and [001] vertical alignments can be equally understood in terms of the C_{ij}.

[15] Finally, it is important to quantify the effect of composition, *x*, on velocities of olivine as a step towards understanding lateral velocity variations in the upper mantle, even though lateral temperature or phase variations are presumed to be their main source. These are usually represented by the seismic parameters:

$$R_{S/P} = \frac{\delta \ln V_S}{\delta \ln V_P}, \qquad R_{\Phi/S} = \frac{\delta \ln V_\Phi}{\delta \ln V_S}. \tag{7}$$

We find that in the 0–20 GPa interval, $R_{S/P}$ in olivine varies between 1.57 and 1.96, while $R_{\Phi/S}$ varies between 0.21 and 0.36. These values fall precisely within the range of these parameters calculated from tomographic studies [*Karato and Karki*, 2001]. This suggests that we cannot unequivocally identify the source of lateral velocity variations at this point. Further and more detailed analyses, e.g. of current and past local conditions, thermochemical equilibrium, etc., appear to be necessary to sort out the source(s) of such velocity anomalies.

4. Conclusions

[16] We investigated the elastic properties of $(Mg_{1-x}, Fe_x)_2SiO_4$ olivine by first-principles to address the effects of iron. We found a tendency for a HS to LS crossover in iron starting at 15 GPa. However, due to the LDA underestimation of transition pressures we restricted iron spin to be in the HS state up to 20 GPa. The true crossover pressure range should start above this. Within this constraint our C_{ij} were found to be consistent with experiments up to 20 GPa. The remaining differences are expected to be fully accounted by temperature effects. We paid particular attention to the artificial effect of the atomic configurations in supercell calculations of elasticity of solid solutions. Different configurations produced C_{ij} within a few percent of each other. However, this effect on aggregate moduli an velocities is very small and negligible for practical purpose. This is a good guidance for future calculations of this kind. Single crystal anisotropies are more sensitive to the atomic configuration. Nevertheless, the overall trends with pressure are reproduced by all configurations. Anisotropies of transversely isotropic aggregates are considerably less dependent on atomic configuration. Compared to other silicates, e.g., $MgSiO_3$ perovskite, whose anisotropy changes drastically with pressure [*Wentzcovitch et al.*, 1998; *Karki et al.*, 2001], anisotropies of olivine showed a weak pressure dependence in the upper mantle. Transverse anisotropy factors were almost pressure independent. In general, our results agree with the weak seismic anisotropy in the upper mantle discussed by *Mainprice et al.* [2005], where experimental results by *Abramson et al.* [1997] are used. Finally, variations of iron in olivine are compatible with the parameters produced by seismic tomography.

[17] **Acknowledgments.** Research supported by NSF/ATM 0428774 and EAR 0810272. Computations were performed at the MSI and LCSE at UMN.

References

Abramson, E. H., J. M. Brown, L. J. Slutsky, and J. Zaug (1997), The elastic constants of San Carlos olivine to 17 GPa, *J. Geophys. Res.*, *102*, 12,253–12,263.

Ceperley, D. M., and B. J. Alder (1980), Ground state of the electron gas by a stochastic method, *Phys. Rev. Lett.*, *45*, 566–569.

Chen, G., B. Li, and R. C. Liebermann (1996), Selected elastic moduli of single crystal olivines from ultrasonic experiments to mantle pressures, *Science*, *272*, 979–980.

da Silva, C., L. Stixrude, and R. M. Wentzcovitch (1997), Elastic constants and anisotropy of forsterite at high pressure, *Geophys. Res. Lett.*, *24*, 1963–1966.

Hazen, R. M. (1976), Effects of temperature and pressure on the crystal structure of forsterite, *Am. Mineral.*, *61*, 1280–1293.

Hohenberg, P., and W. Kohn (1964), Inhomogeneous electron gas, *Phys. Rev. B*, *136*, 864–871.

Irifune, T., T. Shinmei, C. A. McCammon, N. Miyajima, D. C. Rubie, and D. J. Frost (2010), Iron paritioning and density changes of pyrolite in Earth's lower mantle, *Science*, *327*, 193–195.

Karato, S., and B. B. Karki (2001), Origin of lateral variation of seismic wave velocities and density in the deep mantle, *J. Geophys. Res.*, *106*, 21,771–21,783.

Karki, B. B., L. Stixrude, S. J. Clark, M. C. Warren, G. J. Ackland, and J. Crain (1997), Elastic properties of orthorhombic $MgSiO_3$ perovskite at lower mantle pressures, *Am. Mineral.*, *82*, 635–638.

Karki, B. B., L. Stixrude, and R. M. Wentzcovitch (2001), High-pressure elastic properties of major materials of Earth's mantle from first principles, *Rev. Geophys.*, *39*, 507–534.

Kiefer, B., L. Stixrude, and R. M. Wentzcovitch (2002), Elasticity of (Mg, Fe)SiO_3-perovskite at high pressures, *Geophys. Res. Lett.*, *29*(11), 1539, doi:10.1029/2002GL014683.

Kohn, W., and L. J. Sham (1964), Self-Consistent equations including exchange and correlation effects, *Phys. Rev. A*, *140*, 1133–1138.

Liu, W., J. Kung, and B. Li (2005), Elasticity of San Carlos olivine to 8 GPa and 1073 K, *Geophys. Res. Lett.*, *32*, L16301, doi:10.1029/2005GL023453.

Mainprice, D., A. Tommasi, H. Couvy, P. Cordier, and D. J. Frost (2005), Pressure sensitivity of olivine slip systems and seismic anisotropy of Earth's upper mantle, *Nature*, *433*, 731–733.

Musgrave, M. J. P. (1970), *Crystal Acoustics*, 288 pp., Holden-Day, San Francisco, Calif.

Poirier, J. P. (2000), *Introduction to the Physics of the Earth's Interior*, 2nd ed., pp. 15–17, Cambridge Univ. Press, Cambridge, U. K.

Putnis, A. (1992), *Introduction to Mineral Sciences*, 399 pp., Cambridge Univ. Press, Cambridge, U. K.

Rinwood, A. E. (1975), *Composition an Petrology of he Earth's Mantle*, 618 pp., McGraw-Hill, New York.

Rouquette, J., I. Kantor, C. A. McCammon, V. Dmitriev, and L. S. Dubrovinsky (2008), High-pressure studies of $(Mg_{0.9}Fe_{0.1})_2SiO_4$ olivine using Raman spectroscopy, X-ray diffraction, and Mössbauer spectroscopy, *Inorg. Chem.*, *47*, 2668–2673.

Speziale, S., T. S. Duffy, and R. J. Angel (2004), Single-crystal elasticity of fayalite to 12 GPa, *J. Geophys. Res.*, *109*, B12202, doi:10.1029/2004JB003162.

Umemoto, K., R. M. Wentzcovitch, G. Y. Yonggang, and R. Requist (2008), Spin transition in (Mg, Fe)SiO_3, *Earth Planet. Sci. Lett.*, *276*, 198–206.

Vanderbilt, D. (1990), Soft self-consistent pseudopotentials in a generalized eigenvalue formalism, *Phys. Rev. B*, *41*, 7892–7895.

Wallace, D. C. (1972), *Thermodynamics of Crystals*, 484 pp., John Wiley, New York.

Watt, J. P. (1979), Hashin-Shtrikman bounds on the effective elastic moduli of polycrystals with orthorhombic symmetry, *J. Appl. Phys.*, *50*, 6290–6295.

Wentzcovitch, R. M. (1991), Invariant molecular dynamics approach to structural phase transitions, *Phys. Rev. B*, *44*, 2358–2361.

Wentzcovitch, R. M., J. L. Martins, and G. D. Price (1993), *Ab initio* molecular dynamics with variable cell shape: Application to $MgSiO_3$ perovskite, *Phys. Rev. Lett.*, *70*, 3947–3950.

Wentzcovitch, R. M., D. A. Hugh-Jones, R. J. Angel, and G. D. Price (1995), Ab initio study of $MgSiO_3$ C2/c enstatite, *Phys. Chem. Miner.*, *22*, 453–460.

Wentzcovitch, R. M., B. B. Karki, S. Karato, and C. R. S. da Silva (1998), High pressure elastic anisotropy of $MgSiO_3$ perovskite and geophysical implications, *Earth Planet. Sci. Lett.*, *164*, 371–378.

Zha, C.-S., T. S. Duffy, R. T. Downs, H.-K. Mao, and R. J. Hemley (1996), Sound velocity and elasticity of single-crystal forsterite to 16 GPa, *J. Geophys. Res.*, *101*, 17,535–17,545.

Zha, C.-S., T. S. Duffy, R. T. Downs, H.-K. Mao, and R. J. Hemley (1998), Brillouin scattering and X-ray difraction of San Carlos olivine: Direct pressure determination to 32 GPa, *Earth Planet. Sci. Lett.*, *159*, 25–33.

M. Núñez-Valdez, School of Physics and Astronomy, University of Minnesota-Twin Cities, 116 Church St. SE, Minneapolis, MN 55455, USA. (valdez@physics.umn.edu)

K. Umemoto, Department of Geology and Geophysics, University of Minnesota-Twin Cities, 310 Pillsbury Dr. SE, Minneapolis, MN 55455, USA. (umemoto@cems.umn.edu)

R. M. Wentzcovitch, Department of Chemical Engineering and Materials Science, Minnesota Supercomputing Institute, University of Minnesota-Twin Cities, 117 Pleasant St. SE, Minneapolis, MN 55455, USA. (wentzcov@cems.umn.edu)